www.czasopisma.pan.pl PAN POLSKA AKADEMIA NAUK www.journals.pan.pl

A R C H I V E S O F M E T A L L U R G Y A N D M A T E R I A L S

Volume 59 2014 Issue 3

DOI: 10.2478/amm-2014-0156

T. TEKER*, S. KARATAŞ**, S.O. YILMAZ***

MICROSTRUCTURE AND WEAR PROPERTIES OF FeCrC, FeW AND FeTi MODIFIED IRON BASED ALLOY COATING DEPOSITED BY PTA PROCESS ON AISI 430 STEEL

MIKROSTRUKTURA I WŁAŚCIWOŚCI ZUŻYCIA MODYFIKOWANYCH POWŁOK STOPOWYCH NA BAZIE ŻELAZA FeCrC, FeW I FeTi NAKŁADANYCH METODĄ PTA NA STAL AISI 430

The plasma transferred arc (PTA) process was used for developing wear resistance of AISI 430 steel substrate. Appropriate quantities of FeCrC, FeW and FeTi powders were combined to create conditions that synthesized M_7C3 particles into reinforced Fe-based composite surface coating. The phase transformations on new created coated surfaces were comprehensively examined by using a combination of scanning electron microscopy (SEM), microanalysis by energy dispersive spectrometry (EDS), X-Ray diffraction (XRD), microhardness and abrasive wear tests. The microstructure studies of the superficial layers of the coating revealed presence of a mixture of the dendritic phase structure of austenite (γ) and fine eutectic M_7C_3 carbides. The results show that; the concentrations of the elements (Cr, W, Ti) added as ferroalloys, the size of dendrites formed in the coated surface, the change of hardness of the coated surfaces, the carbide volume rate and thickness of the coating changed by the variation of the processing parameters (ratio of reinforcement particulates and heat input).

Keywords: PTA, AISI 430, Surface Coating

Technika PTA została zastosowana do podwyższania odporności na zużycie podłoży ze stali AISI 430. Odpowiednie ilości proszków FeCrC, FeW i FeTi połączono w celu stworzenia warunków, w których syntetyzowane są cząsteczki M_7C_3 zbrojące powłoki kompozytowe na bazie Fe. Przemiany fazowe w nowo utworzonych powłokach zostały szczegółowo zbadane za pomocą kombinacji skaningowej mikroskopii elektronowej (SEM), mikroanalizy spektrometrią dyspersji energii (EDS), dyfrakcji rentgenowskiej (XRD), mikrotwardości i testów ścierania. Badania mikrostruktury wierzchnich warstw powłoki wykazały obecność mieszaniny struktury dendrytycznej austeniu (γ) i drobnych eutektycznych węglików M_7C_3. Wyniki pokazują, że: stężenie pierwiastków (Cr, W, Ti) dodanych jako żelazostopów, wielkość dendrytów utworzonych w powłoce, zmiany twardości powłoki, szybkość objętościowa węglików i grubość powłoki zmieniają się ze zmianą parametrów procesu (stosunek cząstek wzmacniających i mocy cieplnej).

1. Introduction

PTA technique is an apropriate process that can be used for surfac modification of steels by using cheap ferro-alloy powder. During the coating process, the desired composition and a thin surface layer of the substrate material are simultaneously melted which then rapidly solidify to form a dense coating that metallurgically bonds to the base material [1]. PTA process was widely used for the surface treatment of the materials and developed as modification of the plasma arc welding method [1-4]. PTA uses the basic principles used in traditional welding surfacing techniques, and provides a higher deposition rate [1]. The PTA surfacing process is characterized by extremely high temperature, excellent arc stability, low thermal distortion of the part, high coating speeds [5], and the usage of two independent arcs (i.e. non-transferred arc as pilot and transferred arc as main arc) which provide alloying of proper microstructural development [6]. Argon gas passes through cathode and anode and is ionized forming a constricted plasma arc. The ionized gas provides a current path for a transferred arc [5,6]. This technique has a potential to produce rapidly solidifying fine microstructures that exhibit high hardness and increased wear resistance [6-8]. Among the metallic hard coatings produced by PTA, hardness of the iron-chromium-tungsten-titanium alloy coatings is relatively high compared to that of other alloy systems [3,4]. The presence of tungsten in high chromium structures has been found to reduce the fraction of the austenite phase accompanied by the increase in hardness of M_7C_3 carbides. On the other hand, the fraction of austenite phase in microstructure plays an important role in both impact and wears applications [9]. It has been found that primary dendrites, austenite (γ) and M_7C3 carbides develop in Cr-containing microstructures [10]. Materials having high chromium concentration are used in a variety of applications and, the abrasive wear resistance of these materials is high due to hard carbides in the structure [11-13].

* ADIYAMAN UNIVERSITY, FACULTY OF ENGINEERING, DEPARTMENT OF MATERIALS ENGINEERING, 02040, ADIYAMAN, TURKEY
** FIRAT UNIVERSITY, FACULTY OF ENGINEERING, DEPARTMENT OF MATERIALS AND METALLURGICAL ENGINEERING, 23119, ELAZIG, TURKEY
*** NAMIK KEMAL UNIVERSITY, ÇORLU FACULTY OF ENGINEERING, DEPARTMENT OF MECHANICAL ENGINEERING, TEKIRDAĞ/ÇORLU, TURKEY

The alloys having high Cr contents have proeutectic and/or eutectic M_7C_3 carbides in a softer iron matrix. The matrix structure observed most often in the as-cast high Cr alloys is austenite. In addition, the carbides in the structure of these alloys are typically of the M_7C_3 type (M=Fe,Cr). The M_7C_3 carbides generally grow as rods and blades with their long axes parallel to the heat flow direction in the mold [14,15].

Wear resistance is a function of chemical composition, processing conditions, and heat treatment; each alloy system must be evaluated with respect to these variables, as well as the tribological environment [16]. Microstructural parameters for wear resistance of high Cr materials can be conclude as the quantity, orientation, and morphology of carbides, the type of matrix, and the interface between hard phase and the matrix [17]. These parameters can also influence the hardness and fracture toughness. The microstructure of metal matrix composites (MMCs) looks alike to white cast irons. There are two types of foundry methods for making composites with externally added particles, depending on the temperature at which the particles are introduced in the melt. In the liquid metallurgy process [18], the particles are added above the liquidus temperature of the molten alloy. In this processes, a vortex is used, which can form high amount of porosities in the. There are several factors that can influence the quality of the composite product, one very important being the metal melt's ability to wet the ceramic particles. The wettability depends on many parameters: the type of particles, their shape, size, surface roughness and surface chemistry of the outer atomic layers, alloying elements in the melt, the gas environment of the particles when injected into the melt, stirring temperature, and holding the time in the melt. The discontinuously reinforcement phase composites are common due to availability, low cost, independence of mechanical properties from particulate orientation [19], and ease of production via a wide range of manufacturing routes. Titanium will sometimes be added as an inoculant to the high chromium material melts. The free Ti will immediately form small cubic particles of the TiC in the high C-melt. As the rest of the iron starts to solidify, these small particles act as nucleation sites for carbides and austenite. The uses of Ti with W guarantee the nucleation of matrix and carbides at lower temperatures, and enhance the effectiveness of the M_7C_3 carbides [20].

It is the objective of this work to to form a coated surface on AISI 430 steel having homogeniously distributed fine spherical carbides (M_7C_3) formed by inoculation and PTA process in the austenite phase, and to detect the effect of Ti and W on the carbide size and wear resistance.

2. Materials and experimental procedures

AISI 430 samples of 120×50×10 were used as substrates in the PTA processing experiments. A mixture of FeCrC-FeTi-FeW powders were used as alloying powders. The surfaces of the samples were thoroughly cleaned, dried, and ?nally rinsed by acetone. The main chemical composition of FeCrC, FeW, FeTi powders are listed in Table 1, and the ratio of reinforcement particulates used for coating are listed in Table 2.

TABLE 1

Chemical concentration of the powders used for coating (%)

	W	TI	SI	S	FE	CR	C	P
FETI	-	75	0.5	0.03	BAL.	-	-	0.03
FECRC	-	-	1.5	0.04	BAL.	66	7	0.04
FEW	80	-	0.5	-	BAL.	0.5	-	0.04

TABLE 2

Portions of the powders used for coating (%)

SAMPLE NO	FETI %	FEW %	FECRC %
S1	–	–	100
S2.1	10	–	90
S2.2	20	–	80
S2.3	30	–	70
S2.4	40	–	60
S3.1	–	10	90
S3.2	–	20	80
S3.3	–	30	70
S3.4	–	40	60
S4.1	10	10	80
S4.2	15	15	70
S4.3	20	20	60

The average size of the powders was in the range of 40-60 μm. In order to obtain homogeneous mixing, the combined powders were attrition-milled for 1 h using agate ball mill with an agate container, and the balls were operated at 300 rpm. The milled mixture with a thickness in the range of 0.5-2 mm was pre-coated on the surface of the substrate. The experimental conditions employed are also listed in Table 3.

TABLE 3

PTA operating parameters

CURRENT (A)	PLAZMA GAS FLOW (L/MIN.)	SHILDING GAS FLOW (L/MIN.)	TRAVERSE SPEED (MM)	NOZUL DIAMETER (M/MIN.)
130	0.8	20	0.01	3.0

The samples were prepared for metallographic examination by grinding on SiC wheels followed by polishing and etched with a solution having 5 g $FeCl_3$, 30 ml HCl, and 100 ml distilled water. The microstructural evolution was studied by SEM (Model JSM-5310, Japan). EDS was used to study the concentrations of alloying elements in the closed the coatings zone by PTA-process. For XRD analysis, a Rigaku Geigerflex X-ray diffractometer operated at 40 kV and 30 mA using Cu-Kα radiation was used. Microhardness measurements were performed through the thickness of the sample to study the changes in the mechanical properties of the matrix due to plastic deformation by varying the distance to the contact surface. The microhardness distribution measurement method was used to determine the depth of the coatings. A standard microhardness tester, with a Vickers indenter and a 5-g indentation load was used for microhardness measurements of polished surfaces and subsurfaces. The abrasive wear tests were performed using a pin-on disc type apparatus. Abrasive wear tests were carried out under the load of 10, 20 and 30 N on a grade 80 abrasive paper attached to the grinding disc, which rotated at 320 rpm. A fixed track diameter of 160 mm was used in all the tests, and the duration of the abrasion test

TABLE 4

Dimensions and volume portion of carbides

CARBIDES	S1	S2.1	S2.2	S2.3	S2.4	S3.1	S3.2	S3.3	S3.4	S4.1	S4.2	S4.3
VOLUME (%)	40	39.17	43.24	45.94	43	43	41	39	37	41.6	43	47
SIZE (μM)	0.96 7.17	0.55 5.55	0.4 3.1	0.3 2.77	0.27 0.83	0.6 2.5	0.8 3	0.95 3	0.5 3.5	0.9 4	0.6 1.7	0.5 1

was 60 second. Each test was performed with a fresh abrasive paper, and, for each test condition, a minimum of three runs were performed. Wear loses were obtained by determining the masses of the samples before and after wear tests. The wear rates were calculated by converting the mass loss measurements (to the nearest 0.1 mg) to volume loss by using the respective densities:

$$W(mm^3m^{-1}) = \frac{mass\ loss\ (g)/density(gmm^{-3})}{\pi x160x10^{-3}x320(m)}$$

3. Results and discussion

The first group of samples (S_1) was coated by using FeCrC powders. The Figure 1 shows the SEM micrograph of the superficial layer, and the boundary between the melted and substratemetal of sample $S_{1.1}$. Results noted in Table 4 reveal the role played by PTA processing parameters on the coating dimensions, carbide vol.%, carbide size and hardness of the coating.

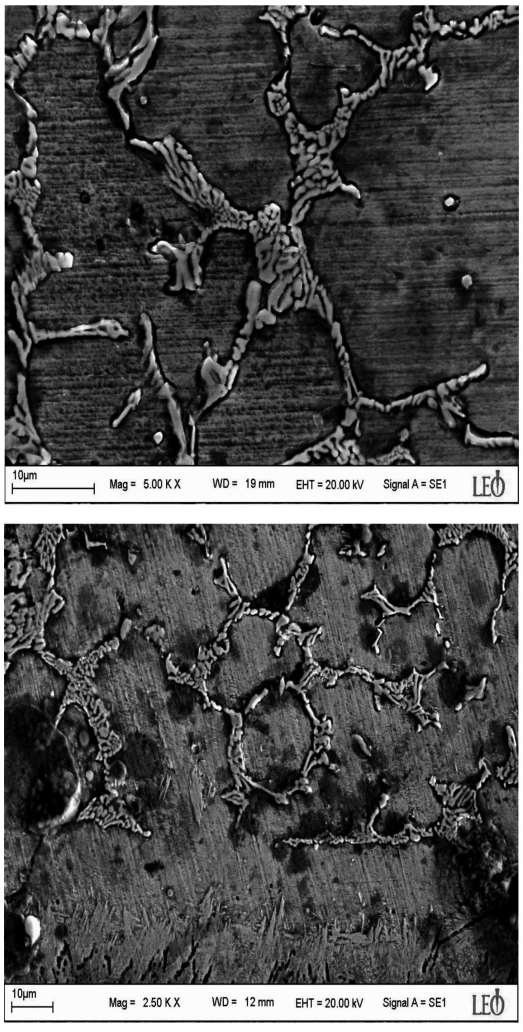

Fig. 1. SEM micrograph of sample S_1 **a)** X500, **b)** X250

The microstructure of the carbides and matrix is shown in Figure 1, where the M_7C_3 carbides are in intergranular form, and the microstructure is in the form of an eutectic ($M_7C_3+\gamma$) phase mixture (Table 4). EDS analyses of the matrix and the carbides are given in Table 5, from which it can be seen that the carbides are stochiometrically in the form of M_7C_3. Figure 2 shows representative XRD results of sample S1 that reveal the effect of PTA processing parameters on the phases present in the coating microstructures containing FeCrC powders. The presence of M_7C_3 diffraction peaks is clearly visible and indicating the formation of M_7C_3 carbides in austenite (γ) phase.

TABLE 5

EDS analysis taken from the coated surface of sample S_1

	POINT	C	SI	CR	FE
MATRIX	(WT.%)	0.94	1.39	19.90	48.75
CARBIDE	(WT.%)	4.05	0.23	46.56	49.16

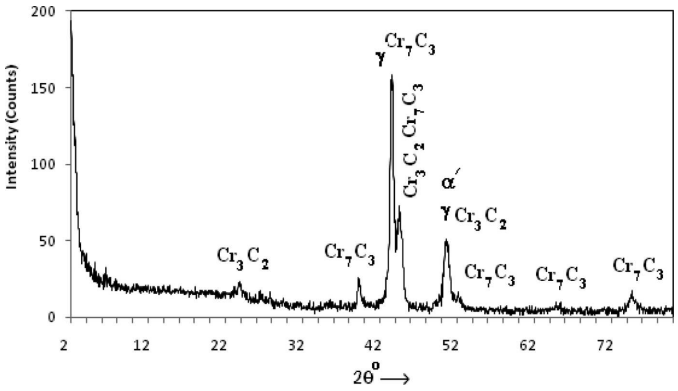

Fig. 2. XRD result of sample S_1

Titanium was added to cladding powders as FeTi for morphological change of carbides, and this group was designated as second group. The carbide size and vol.% parameters corresponding to the second group show that increasing FeTi rate in the cladding powder bring about a serious decrease in the carbide size (Table 4). The primary phases were seen to become relatively small, which means increasing the titanium rate in caladding powders increases nucleation rate of carbides in microstructures. EDS analyses of carbides of sample $S_{2.1}$ (Table 6) show that the Fe/Cr ratio is in the range of 3.5-4.0, which suggests that the carbide structure is probably $(Cr_2Fe_7)C_3$ [22].

TABLE 6

EDS analysis taken from the surface of sample $S_{2.1}$

	POINT	C	SI	CR	FE	TI
MATRIX	(WT.%)	1.23	1.04	18.00	79.49	0.24
CARBIDE	(WT.%)	4.30	0.95	19.53	75.78	0.43

The hardness of the M_7C_3 carbides increases with Cr content of carbide [22]. The relationship between Cr content and M7C3 carbide hardness provides insight into the abrasion performance of the coated surface. It is clearly, higher Cr concentration produces harder M_7C_3 carbides [20-23]. It is seen form the EDS analyses that the carbides of the sample $S_{2.1}$ contain 0.43 wt.% Ti, and the increase of the Ti in cladding powders increased Ti wt.% and decreased Cr concentration of carbides. The variation of the microhardness for sample $S_{2.1}$ and $S_{2.4}$ was interpreted in Table 7.

TABLE 7

Microhardness of the carbides and matrix of the samples

SAMPLE NO 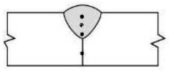	**MATRIX HARDNESS (H_V)**				**CARBIDE HARDNESS (HV)**
S1.1	726.3	780.5	759.3	645.9	2400
S2.1	896.9	830.3	849.7	650.5	1830
S2.2	721.2	653.2	727.3	543.2	1350
S2.3	810	903.2	947.8	775.9	1050
S2.4	735.2	724.4	705.6	582.4	1250
S3.1	875.1	850.5	701.3	720.7	–
S3.2	875.5	878.3	653.2	750.5	960
S3.3	865.2	746.5	713.8	678.4	1700
S3.4	905	857.2	728.2	645.2	–
S4.1	828	839.8	775	708.7	–
S4.2	758.7	724.6	865.6	708.6	1250
S4.3	953.3	965	894	775.5	1250

The microhardness values confirm that significant surface hardening was achieved by PTA process, and the microhardness fall from surface to the substrate (Table 7). The variations ranging from 775-1050 H_V for sample $S_{2.3}$ should be attributed to the presence of large carbides in the microstructure (Table 4). Conversely, the microhardness values of the refined microstructure of sample $S_{2.2}$ obtained at a lower powder feed rate and heat input exhibits fewer variations in hardness. The eutectic microstructures as well as the size of carbides and the spacing between the intergranular carbides depend on the solidification rate [24]. Besides, intergranular structures can form at relatively lower solidification rates. Therefore, the higher hardness of the sample $S_{2.3}$ is related to the lowere size of the austenite phase. On the other hand, the lower hardness variation of sample $S_{2.2}$ may be associated with the high ratio of austenite phase in the primary dendrites (Figure 3-6).

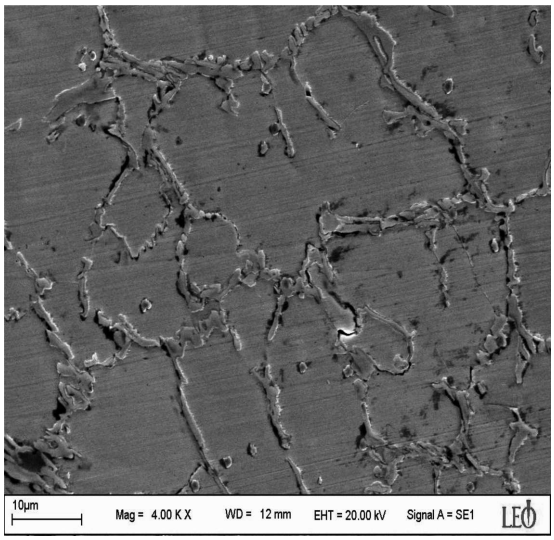

Fig. 3. SEM micrograph of sample $S_{2.1}$

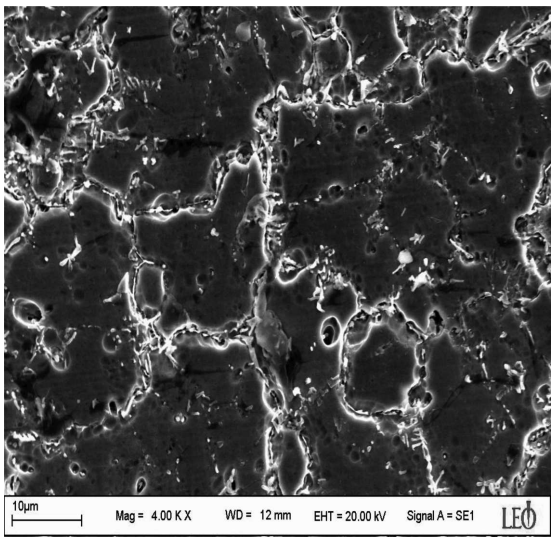

Fig. 4. SEM micrograph of sample $S_{2.2}$

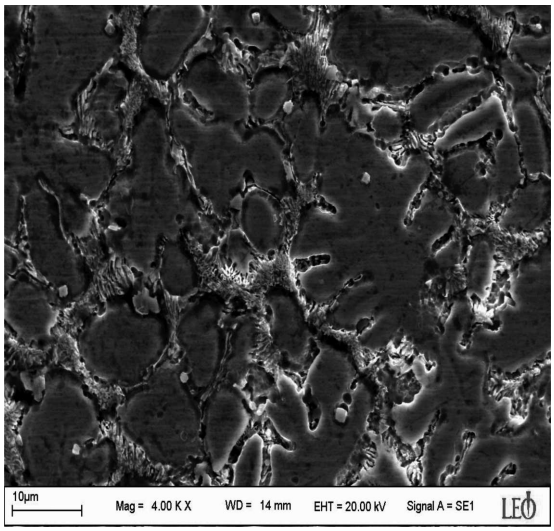

Fig. 5. SEM micrograph of sample $S_{2.3}$

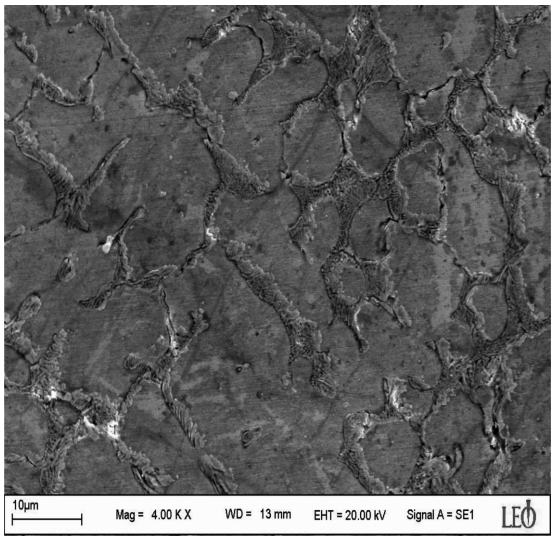

Fig. 6. SEM micrograph of sample $S_{2.4}$

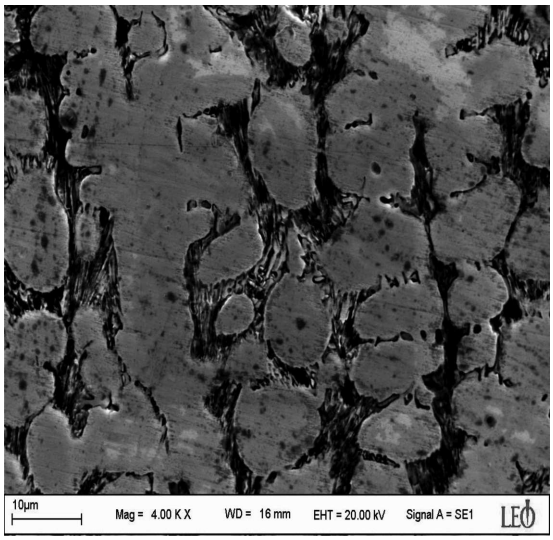

Fig. 7. SEM micrograph of sample $S_{3.1}$

The microhardness variation of samples $S_{2.1}$, $S_{2.2}$, $S_{2.3}$ and $S_{2.4}$ are compared, which shows that a marked enhancement of the coating hardness occurs due to the microstructural refinement. Table 8 shows the changes in chemical composition of superficial layers of the samples coated by FeCrC-FeTi alloy powders, where the increase of the Ti concentration in cladding powders increased the Ti wt.% in carbide and matrix together, and decreased the Cr wt.% of the carbides from 65.67 wt% to 19.98wt%.

TABLE 8
EDS analysis taken from the coated surface of sample $S_{2.2}$-$S_{2.4}$

	SAMPLE	C	CR	FE	TI
MATRIX	$S_{2.2}$	1.91	17.70	80.09	0.80
	$S_{2.3}$	1.43	19.16	78.81	1.33
	$S_{2.4}$	1.13	19.82	77.59	1.45
CARBIDE	$S_{2.2}$	5.18	65.67	28.25	0.90
	$S_{2.3}$	3.35	26.79	67.78	2.08
	$S_{2.4}$	2.48	19.98	74.94	2.60

For the third group of the samples, W was added to the cladding powder mixture as FeW. Figure 7-10 show the formation of matrix, primary dendrites and eutectic structure formed in the interdendritic regions for samples $S_{3.1}$-$S_{3.4}$. From the micrographs it is seen that the microstructure is in the form of hypoeutectic type. The carbides occured as primary dendrities, and the matrix appeared as interdendritic form having a thickness of aproximately 5 μm. The EDS analyses of the matrix and carbides are interpreted in Table 9. The resultant carbide can be abbreviated as $((FeCrW)_3C)$ depending on the Fe/Cr ratio [19]. Figure 11 interprets the XRD result of the sample $S_{3.4}$, which reveals that the major phase is austenite (γ), and the minor phase is $((FeCrW)_3C)$. The addition of the W to the coating powders raised the carbide concentration and the size of the carbides, and the increase of W in the coating powders caused to increase of Cr wt.% of carbides together with Wwt% (Table 9).

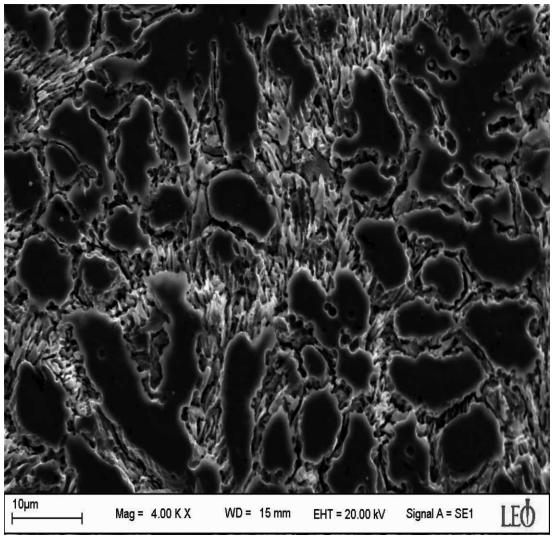

Fig. 8. SEM micrograph of sample $S_{3.2}$

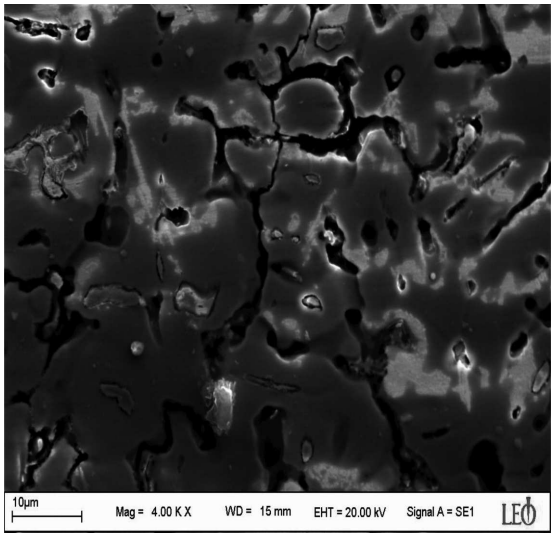

Fig. 9. SEM micrograph of sample $S_{3.3}$

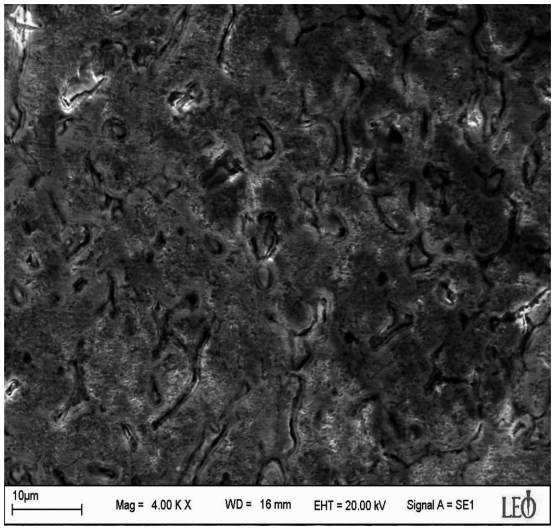

Fig. 10. SEM micrograph of sample $S_{3.4}$

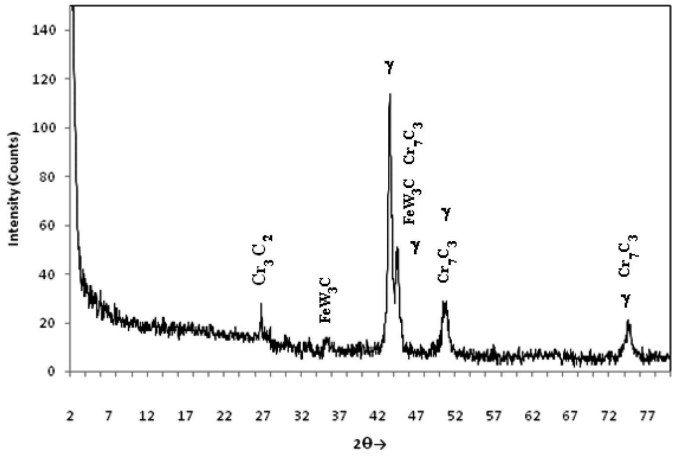

Fig. 11. XRD result of sample $S_{3.4}$

TABLE 9
EDS analysis taken from the coated surface of sample $S_{3.1}$-$S_{3.4}$

	SAMPLE	C	CR	FE	W
MATRIX	$S_{3.1}$	0.79	16.70	78.06	4.44
	$S_{3.2}$	0.85	17.42	74.98	5.02
	S_{33}	0.93	18.05	75.97	5.05
	$S_{3.4}$	1.16	19.47	74.31	5.06
CARBIDE	$S_{3.1}$	13.12	18.45	63.25	5.18
	$S_{3.2}$	9.22	18.42	67.35	5.02
	S_{33}	7.32	20.77	67.06	5.85
	$S_{3.4}$	5.79	34.83	52.28	6.11

FeTi powders were added to the coating powders together with FeW and FeCrC for the fourth group of the samples. The change on the carbide vol.%, and size for sample S4.1- S4.3 are interpreted in Table 4. The stability of the matrix is important during the wear process [25]. Hence, Ti was added with W to stable the austenite phase. Table 10 notes the change of chemical composition of superficial layer as EDS analyses of the carbide and matrix. The presence of Ti with W in cladding powders forms a carbide having high amount of Cr, and the increase of Ti increased the Cr concentration and microhardness of the carbides.

Figure 12-15 shows that the addition of FeTi powder promotes the formation of refined dendrites. It is thought that an interdendritic eutectic occurs, when the microstructure have Ti together with W and Cr compared with samples S2 and S3 groups. Consequently, the size of the carbides decreases. The microhardness results obtained for samples $S_{4.2}$ and $S_{4.3}$ are shown in Table 4. The resultant, Fe-Cr carbide can be abbreviated as (M_3C) from the Fe/Cr ratio (Table 10) [19]. Results of the present study reveal the occurrence of two basic structures both of which depend on the PTA processing parameters and associated alloy compositions. The first, is the formation that results in the primary dendrites of γ (fcc) and the eutectic consisting of γ and hcp WCrC intermetallic phases. The mechanism of the second structure involves the formation of M_7C_3 carbides and eutectic γ and hcp M_3C carbides. Figure 13 shows representative XRD results that reveal the effect of Cr-W-Ti-C on the phases present in the surfaces of the coating microstructures (e.g. increase in intensity of austenite phase). The XRD results also confirm that the addition of Ti leads to formation of eutectic structures containing austenite and WCrC phase mixture with M_7C_3 carbides.

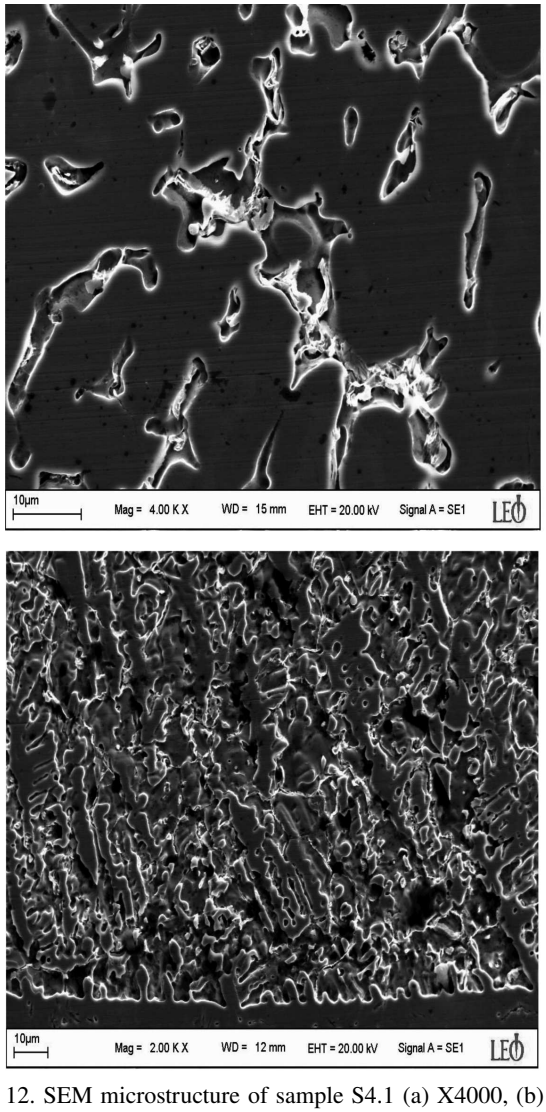

Fig. 12. SEM microstructure of sample S4.1 (a) X4000, (b) X2000

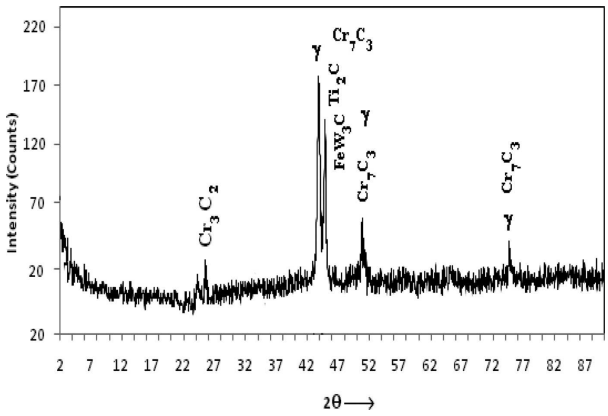

Fig. 13. XRD result of sample $S_{4.1}$

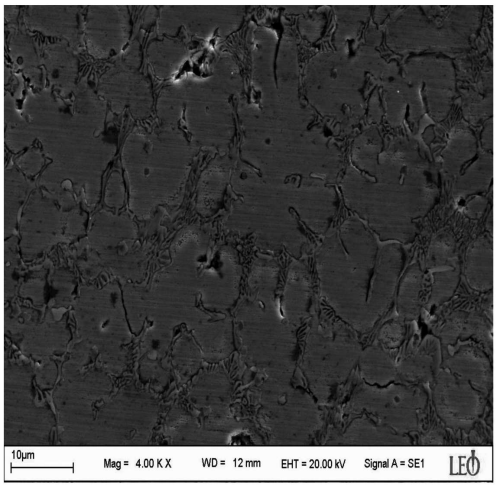

(a)

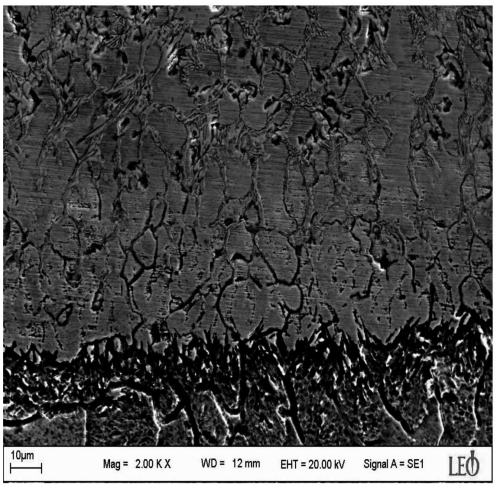

(b)

Fig. 14. SEM microstructure of sample $S_{4.2}$, (a) X4000, (b) X2000

TABLE 10

EDS analysis taken from the coated surface of sample $S_{4.1}$-$S_{4.3}$

	SAMPLE	C	CR	FE	W	TI
MATRIX	$S_{4.1}$	1.22	16.15	74.36	4.12	0.19
	$S_{4.2}$	1.60	18.11	75.40	4.44	0.45
	$S_{4.3}$	2.59	18.31	73.79	4.97	0.34
CARBIDE	$S_{4.1}$	5.48	15.99	78.38	4.11	0.30
	$S_{4.2}$	3.92	56.89	33.08	5.04	0.77
	$S_{4.3}$	4.11	50.85	38.68	4.99	1.42

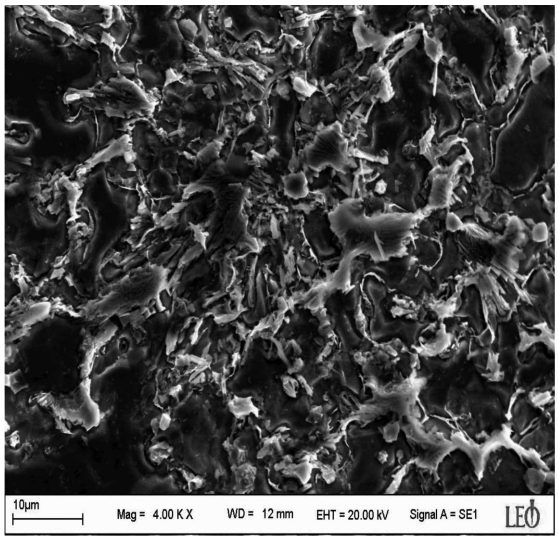

(a)

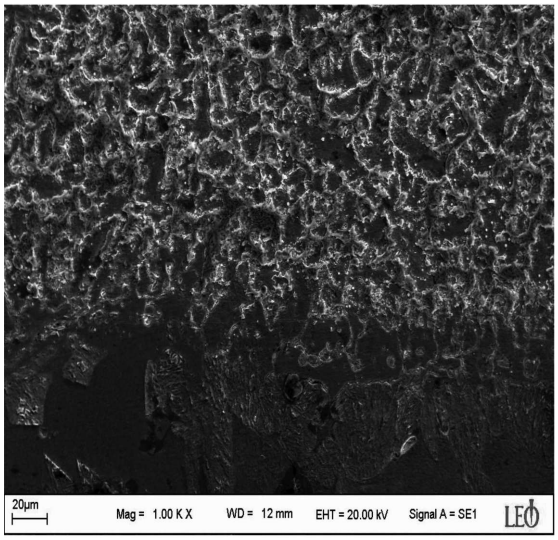

(b)

Fig. 15. SEM microstructure of sample $S_{4.3}$, (a) X4000, (b) X2000

3.1. Wear tests

Figure 16 shows the wear rate for different surface treated samples as a function of the test load, and the wear rate increases with the test load for all surface treated samples. The FeCrC, FeTi and FeW additions had systematic effect on wear rate, respective of load. For the FeTi additions, very similar wear values were found in all the samples for each load. The sample $S_{2.4}$ exhibited the greatest wear resistance. In contrast, the reference sample $S_{1.1}$ systematically exhibited the worst wear resistance, followed by the coated surface having FeCrC.

Results indicate that FeCrC, FeW and FeTi alloying improve the wear resistance of the steel surface compared to the unreinforced sample. The variation of the microhardness of FeCrC, FeCrC-FeTi, FeCrC-FeW and FeCrC-FeTi-FeW coated samples with wear rate are interpreted in Figure 17.

In the Figure 17, it is seen that the relationship between microhardness and wear rate is in the form of polinomic function. Wear rate is a function of chromium, titanium and wolfram concentration of the carbides. From Figure 17, also it is seen that the increase at volume concentration and morphology of carbide increased hardness and decreased the wear rate in considerable amount. The results demonstrate that the wear

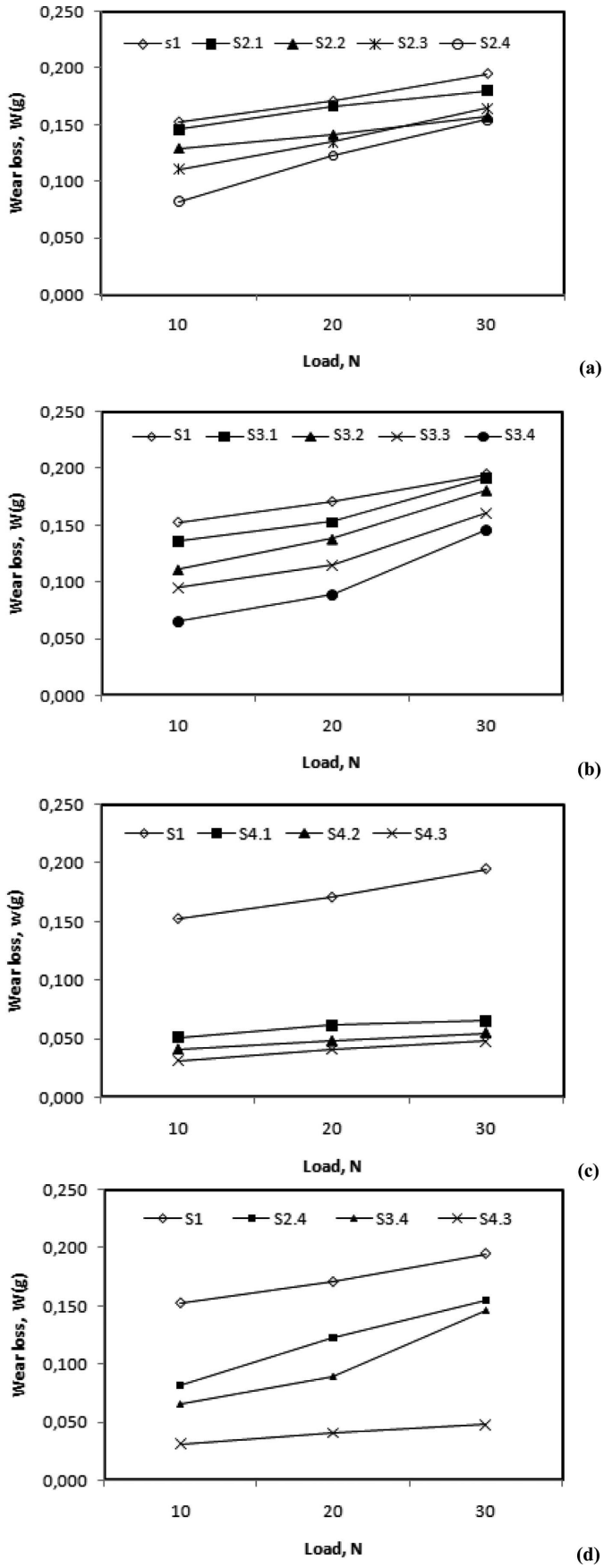

Fig. 16. Wear loss versus load for a sliding distance of 800 m and a sliding speed of 0.84 m s^{-1}

loss and hardness is not proportional for all of the samples. The wear loss of the samples having titanium decreased with hardness. On the other hand, the wear loss and hardness of the samples having wolfram changed inversely and between the different coated surfaces the wear rate of the S4 group samples is the most sensitive against hard phase volume percentage. The wear loss of the coated surfaces, which can be renamed as MMC composite, increase linearly through the entire applied load range.

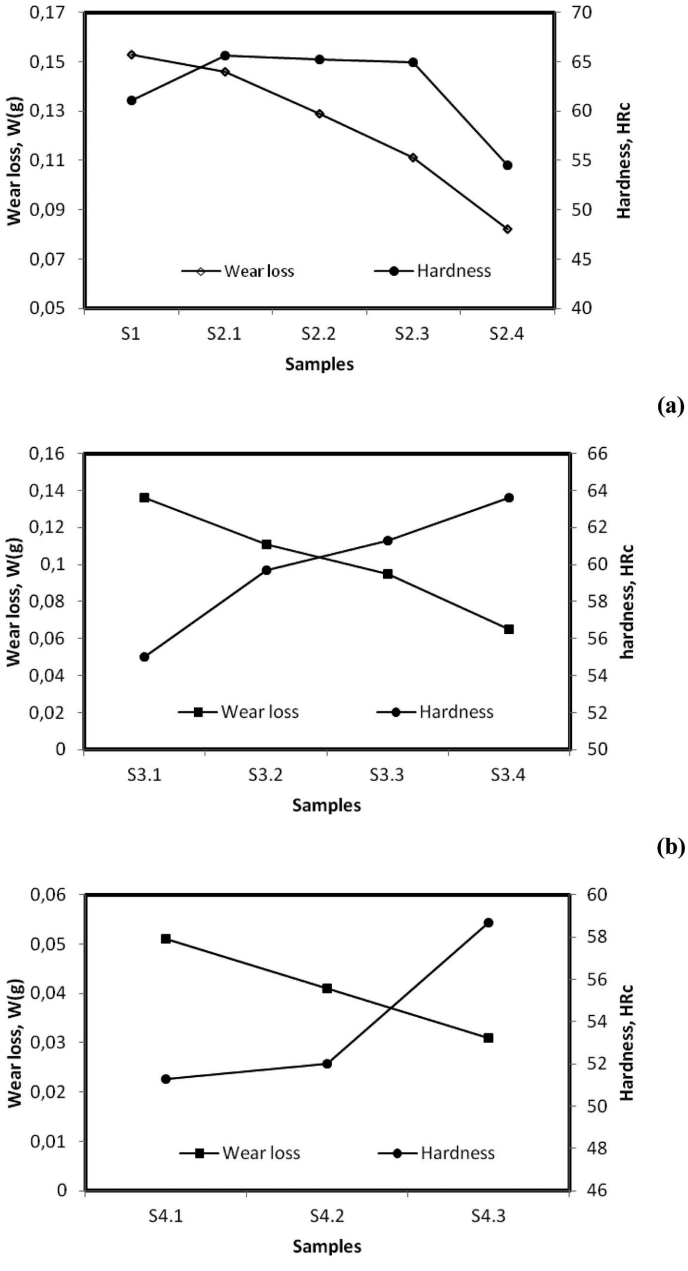

Fig. 17. The relationship between wear loss and hardness of the samples, (a) 2. Group, (b) 3. Group, (c) 4. Group

4. Conclusion

1. Four different coated surface microstructures were produced by adding FeCrC, FeW and FeTi powders. These microstructures were classified based on powder concentration. It was concluded that the formation of microstructures depends mainly on carbon concentration and Fe/Cr

ratio of coated surface layers. The matrix phase is face centered cubic (fcc) austenite (γ) and the reinforcement phase is M_7C_3 (M= Cr, Fe) carbide in interdendritic form.

2. Carbon and chromium concentration of the coated surface decreases going down from the surface to the steel substrate, which is thought to be due to termal gradient. Probably increasing carbon and chromium contents reduces the eutectic reaction temperature and solidification rate of the eutectic point.
3. The presence of the W together with Cr, raises the size and concentration of the MC_3 carbides.
4. The variation of the microhardness of FeCrC, FeCrC-FeW, FeCrC-FeTi and FeCrC-FeW-FeTi coated samples relationships with wear loss, revealed as their form of polinomic function. In addition, the wear rate curves represent that the wear rate changes with hardness and the load in a polinomic function.

REFERENCES

[1] R.L. Deuis, J.M. Yellup, C. Subramanian, Metal-matrix composite coatings by PTA surfacing, Compos. Sci. Technol. **58**, 299 (1998).
[2] L.P. Connor, Welding Handbook. (eighth ed.), American Welding Society, Miami, FL **1**, 11 (1987).
[3] E. Bourithis, A. Tazedakis, G. Papadimitriou, A study on the surface treatm ent of "Calmax" tool steel by a plasma transferred arc (PTA) process, J. Mater. Process. Technol. **128**, 169 (2002).
[4] M. Yan, An experimental study of the remelting of an Fe-C-Cr-Si-B overlay with a micro beam plasma arc, Surf. Coat. & Technol. **99**, 132 (1998).
[5] Y.F. Liu, J.S. Mu, X.Y. Xu, S.Z. Yang, Microstructure and dry-sliding wear properties of TiC-reinforced composite coating prepared by plasma-transferred arc weld-surfacing process, Mater. Sci. & Eng. A. **458**, 366-370 (2007).
[6] S. Schreck, K.H. Zum Gahr, Laser-assisted structuring of ceramic and steel surfaces for improving tribological properties, Applied. Surf. Sci. **247**, 1-4, 616-622 (2005).
[7] L.W. Tsay, Z.W. Lin, R.K. Shiue, C. Chen, Hydrogen embrittlement susceptibility of laser-hardened 4140 steel, Mater. Sci. & Eng. A. **290**, 46-54 (2000).
[8] X.B. Tian, Z.M. Zeng, T. Zhang, B.Y. Tang, P.K. Chu, Medium-temperature plasma immersion-ion implantation of austenitic stainless steel, Thin Solid Films **366**, 1-2, 150-154 (2000).
[9] A. Matthews, A. Leyland, K. Holmberg, H. Ronkainen, Design aspects for advanced tribological surface coatings, Surf. Coat. & Technol. **100-101**, 1-6 (1998).
[10] W. Xiaolei, C. Guangnan, Nonequilibrium microstructures and their evolution in a Fe-Cr-W-Ni-C laser clad coating, Mater. Sci. & Eng. A. **270**, 2, 183-189, (1999).
[11] K.M. Kulkarni, V. Anand, Metals Handbook, 9^{th} ed., ASM, Metals Park, OH **7**, 823-836 (1984).
[12] A.B. Kinzel, W. Crafts, The alloys of iron and chromium, Mc Graw-Hill, New York, NY, I: 25-45 (1937).
[13] A.B. Kinzel, R. Franks, The alloys of iron and chromium, Mc Graw-Hill, New York, NY, II: 173-227 (1937).
[14] F. Maratray, Choice of appropriate compositions for chromium-molybdenum white irons, AFS Trans. **79**, 121-124 (1971).
[15] J.L. Parks, Characteristics of as-cast and subcritically heat-treated high-chromium-molybdenum white irons for thick-section castings, AFS Trans. **86**, 93-102 (1978).
[16] K.H. Zum gahr, D.V. Doane, Optimizing fracture toughness resistance in white cast irons, Metal. Trans. A. **11A**, (1980) 613-20.
[17] K.H. Zum gahr, G.T. Eldis, Abrasive wear of white cast irons, Wear **64**, 175-94 (1980).
[18] R. Mehrabian, M.C. Flemings, New trends in materials processing, ASM, Metals Park, 98 (1976).
[19] L.D. Mcdanels, Analysis of stress-strain, fracture, and ductility behavior of aluminum matrix composites containing discontinuous silicon carbide reinforcement, Metal. Trans. **16A**, 1105 (1985).
[20] J.M. Sanchez, I. Azcona, F. Castro, Mechanical properties of titanium diboride based cermets, J. Mater. Sci. **35**, 9-14 (2000).
[21] G. Laird, R. Gundlach, K. Rohrig, Abrasion-resistant cast iron handbook, 1st ed, American Foundry Society, Des. Plaines, IL, (2000).
[22] S.O. Yılmaz, Wear behavior of TiB_2 inoculated 20Cr-3Mo-4C high chromium white cast irons, J. Mater. Sci. **42**, 6769-6778 (2007).
[23] J. Zhang, A.T. Alpas, Delamination wear in ductile materials containing second phase particles, Mater. Sci. & Eng. A. **160** (1), 25-35 (1993).
[24] R. Trivedi, W. Kurz, Proc. Symp. Solidification processing of eutectic alloys, D. Stefanescu, G.J. Abbaschian, R.J. Bayuzick, eds., TMS-AIME, Warrendale, PA, 3-34 (1988).
[25] S. Gnyusov, S. Tarasov, Y. Ivanov, V. Rothstein, The effect of pulsed electron beam melting on microstructure, friction and wear of WC-Hadfield steel hard metal, Wear **257**, 97-103 (2004).

Received: 10 December 2013.